Percent Infarct Mapping: An R_1-Map-Based CE-MRI Method for Determining Myocardial Viability Distribution

Pál Surányi,[1,4] Pál Kiss,[1] Brigitta C. Brott,[2] Tamás Simor,[1,4] Ada Elgavish,[3,4] Balázs Ruzsics,[1] Nada H. Saab-Ismail,[4] and Gabriel A. Elgavish[1,2,4*]

Viability detection is crucial for the management of myocardial infarction (MI). Signal intensity (SI)-based MRI methods may overestimate infarct size in vivo. In contrast to SI, the longitudinal relaxation-rate enhancement (ΔR_1) is an intrinsic parameter that is linearly proportional to the concentration of contrast agent (CA). Determining ΔR_1 in the presence of an infarct-avid persistent CA (PCA) allows determination of the per-voxel percentage of infarcted tissue. Introduced here is a ΔR_1-based CE-MRI method, termed percent infarct mapping (PIM), for quantifying myocardial viability following delayed PCA accumulation. In a canine MI model ($N = 6$), PIMs were generated using a persistent CA (PCA) and validated using triphenyltetrazolium-chloride (TTC) histochemistry. Voxel-by-voxel R_1 maps of the entire left ventricle (LV) were generated 24 and 48 hr after PCA administration using inversion recovery (IR) with multiple inversion times (TIs). PI values were calculated voxel by voxel. Significant correlations ($P < 0.01$, $R = 0.97$) were obtained for PI per slice (PIS) determined using PIM vs. corresponding TTC-based values. Median deviations of PIS with PIM from that with TTC were only 1.01% and −0.53%, at 24 hr and 48 hr. Median deviations from the true infarction fraction (IF) were 1.23% and 0.49% of LV at 24 hr and 48 hr, respectively. No significant difference was found between $PIM_{24\ hr}$ and $PIM_{48\ hr}$. ΔR_1-based PIM is an accurate and reproducible method for quantifying myocardial viability distribution, and thus enhances the clinical utility of CE-MRI. Magn Reson Med 56:535–545, 2006. © 2006 Wiley-Liss, Inc.

Key words: MRI; contrast agent; MI; myocardial viability; canine

Detection of viability is crucial for the management of myocardial infarction (MI). An accurate method that could distinguish irreversible injury from myocardial hibernation or stunning would be useful for making clinical decisions (1,2). Patients with remaining viable tissue in ischemically injured regions benefit most from revascularization (3,4). When an imaging method overestimates the true size or transmurality of the infarct, revascularization may be deemed unnecessary for patients who, in truth, could benefit from it.

Contrast-enhanced magnetic resonance imaging (CE-MRI) offers high-in-plane-resolution determination of infarct size, aided by the delayed accumulation of certain agents in the infarcted tissue. The delayed enhancement method of CE-MRI has been used widely to determine infarct size (5–13). Nevertheless, there has been criticism regarding quantification, and some investigators have found that the delayed-enhancement method may overestimate infarct size in vivo (14–20). Recently various novel techniques have been developed in an effort to circumvent the potential problems of finding the optimum threshold for infarcted vs. viable tissue (21–23). Even among these techniques, however, major methodological differences remain, and to date none have been universally accepted as optimal.

Contrast agent (CA)-induced signal intensity (SI) enhancement depends nonlinearly on the CA concentration in the myocardial volume element imaged. SI enhancement is not an intrinsic physical parameter, but depends on the pulse sequence, acquisition parameters, and field inhomogeneity. The intrinsic physical parameter, enhanced in linear proportion with CA concentration, is the relaxation rate enhancement, ΔR_1, which is the difference between $1/T_1$ in the presence vs. the absence of CA (24). Using ΔR_1 liberates the quantification of infarct size from dependence on extraneous experimental factors (field inhomogeneity, preparation-pulse error, saturation, T_2 effects etc.). The ΔR_1 obtained from a given myocardial volume element (voxel associated with a given pixel in the MR image) estimates the volume of infarcted tissue to within 1% of a simulated value (see Appendix). Thus, a 3D ΔR_1-map of the left ventricle (LV) is a faithful representation of infarct distribution with a voxel-by-voxel resolution.

At the basis of our approach is the fact that voxels that are in neither the remote nor the core infarct regions have a mixed nature—neither entirely healthy nor entirely infarcted (see Materials and Methods). Therefore, each voxel will have a heterogeneous CA concentration. The effects of infarction, such as the distribution of intra- and extracellular water, as well as the concentration of CA will be proportional to the percentage of infarction. Therefore, ΔR_1 will also vary spatially in a manner proportional to the local percentage of infarction. As a result, this method can determine a continuum of the extent of infarct that exists in the different voxels, as opposed to providing the all-or-

[1]Department of Biochemistry and Molecular Genetics, University of Alabama at Birmingham, Birmingham, Alabama, USA.

[2]Department of Medicine, Division of Cardiovascular Disease, University of Alabama at Birmingham, Birmingham, Alabama, USA.

[3]Department of Genetics, University of Alabama at Birmingham, Birmingham, Alabama, USA.

[4]Elgavish Paramagnetics Inc., Birmingham, Alabama, USA.

*Correspondence to: Gabriel A. Elgavish, Ph.D., Department of Biochemistry and Molecular Genetics, University of Alabama at Birmingham, MCLM 556, Birmingham, AL 35294-0005. E-mail: gabi@uab.edu

Grant sponsor: NIH; Grant numbers: R44 HL58285; RO1 HL63340.

Presented at the 13th Annual Meeting of ISMRM, Miami Beach, FL, USA, 2005.

Received 2 September 2005; revised 27 April 2006; accepted 2 May 2006.

DOI 10.1002/mrm.20979

Published online 4 August 2006 in Wiley InterScience (www.interscience.wiley.com).

none results of the delayed-enhancement method presently used in the clinic.

Infarct-avid CAs distribute into all myocardial voxels in proportion with the per-voxel percentage of infarcted, irreversibly damaged cells. Thus the ΔR_1-map transforms into a percent-infarct map (PIM) of the heart (see Materials and Methods). For each voxel we derive a single number, the PI value that reflects the percentage of infarcted cell mass. A PIM is a map of the PI values of all voxels, obtained from the cardiac MR images, and it assesses not only the infarction fraction (IF), but also the density of infarct with a resolution governed by the minimum achievable voxel size.

As a general rule, R_1 can be determined most accurately by an inversion-recovery (IR) acquisition sequence using multiple inversion times (TIs). Also, the R_1 of a voxel should not vary significantly in the course of such an IR acquisition. The total time frame for such R_1 determinations, using the technique described by Messroghli et al. (25), with the number of tomographic slices necessary to cover the LV myocardium is 30–40 min. Thus, R_1 mapping, when using such slow acquisition techniques, can be carried out only with a CA that is sufficiently long-lived in the myocardium to maintain its concentration during 30–40 min within limits that are not larger than the experimental error of R_1 measurements. We call such a CA a persistent CA (PCA). For several years now we have been developing myocardial CAs that are appropriate for the diagnosis of ischemic heart disease (26–31). Although Gd-(ABE-DTTA), which is still in the investigational phase, was used in this study as a PCA because of its slow tissue kinetics and infarct avidity (32–34), fast methods for R_1 measurement have recently emerged (35). Once these fast R_1-mapping methods become commercialized, other CAs with shorter tissue lifetimes may be also employed to generate PIMs. Thus the PIM method, in principle, is independent of the R_1 acquisition technique and the particular infarct-avid CA used to generate the R_1 map.

In this work we demonstrate the feasibility and validation of PIM, using this infarct-avid PCA in a canine model of reperfused infarction. The results were compared with triphenyltetrazolium-chloride (TTC) staining, an established postmortem tool for determining infarct size. TTC staining was formerly validated with microscopic histology and has been used widely as a validation technique for MRI results (8,14,15,19,36–38).

MATERIALS AND METHODS

Canine Model

Our studies were approved by our IACUC and complied with the *Guidelines for the Care and Use of Laboratory Animals* (NIH). Male hounds (18–20 kg, $N = 6$) were anesthetized with ketamine (5.0 mg/kg) and diazepam (0.5 mg/kg) I.V. Following intubation, anesthesia was maintained by continuous administration of isoflurane (2.5–3%V/V). Fentanyl (50–100 μg I.V. every 30 min) was used for analgesia. Heparin was introduced intravenously as needed to maintain activated blood-clotting time above 300 s. A 2–4-mm angioplasty balloon was introduced into the LAD or the LCx, inflated, and left in position for 180 min to produce MI. After the balloon catheter was removed, coronary angiography was repeated to confirm reperfusion.

PCA

Gd(ABE-DTTA) was synthesized and an injectable sample was prepared as described by Saab-Ismail et al. (27). PCA (0.05 mmol/kg Gd(ABE-DTTA)) was administered intravenously, 48 hr after reperfusion.

Gd(ABE-DTTA) has a molecular weight of 759.8 Daltons, an aqueous solubility of 25 mM, and a longitudinal relaxivity of 18.51 $s^{-1}mmol^{-1}$ at 1.5T (27,39). The physiological effects of the MRI-effective dose (0.05 mmol/kg) of Gd(ABE-DTTA) were investigated in dogs with MI ($N = 8$ for 48 hr, $N = 4$ for 8 weeks) by monitoring blood parameters (Ruzsics et al., *Pharmacology,* in press). No significant changes were detected, except for a transient increase exceeding the normal range in alanine-aminotransferase (ALT) activity in the short-term group at 24 and 48 hr after agent administration, as expected due to isoflurane anesthesia.

In a previous study (32) we showed that accumulation of Gd(ABE-DTTA) in the infarct becomes detectable at 2 hr ($R_1 = 1.88\ s^{-1}$) and R_1 is still at the enhanced level of $1.9s^{-1}$ 144 hr after PCA administration, although the agent is essentially cleared from the bloodstream in 5 days. The rate of change in myocardial R_1 was less than 1% per hour throughout the first week.

MRI

A 1.5T GE Signa-Horizon CV/i was used for cardiac MRI. The dogs were anesthetized for MRI as above. Forty-eight hours after reperfusion, R_1 maps were obtained to determine precontrast R_1 in myocardium ($R_{1,0}$) to confirm that our R_1-mapping method yielded accurate R_1 values and to provide a control for determination of ΔR_1. Inversion-recovery (IR) images were generated using a standard gated, IR-prepared, segmented, fast-gradient-echo sequence with varying TIs, as described by Messroghli et al. (25). The imaging parameters were as follows: FOV = 300 mm, image-matrix = 256 × 256, slice thickness = 10 mm, flip angle = 25°, echo time (TE) = 3.32 ms, views per segment = 16, and repetition time (TR) = 1500–2400 ms (three cardiac cycles, constant throughout a given R_1-mapping procedure). Eight to 10 TIs were used, ranging from 200 to 1200 ms. Image acquisition was timed to the same end-diastolic phase to allow pixel-by-pixel analysis (25). The entire LV was covered with six short-axis slices. The apex was visualized in the long-axis three-chamber view. Scan time (breath-hold) per image was 15–20 s.

Following the acquisition of the control R_1 maps, PCA was administered. At 24 hr and 48 hr after PCA, R_1 maps were obtained for the purpose of PIM ($PIM_{24\ hr}$ and $PIM_{48\ hr}$).

Image Processing and Generation of the PIM

ImageJ was used to import images as stacks. Accurate coregistration of images with different TIs was confirmed by the lack of displacement when the stacks were viewed as movies. On the short-axis images the endo- and epicar-

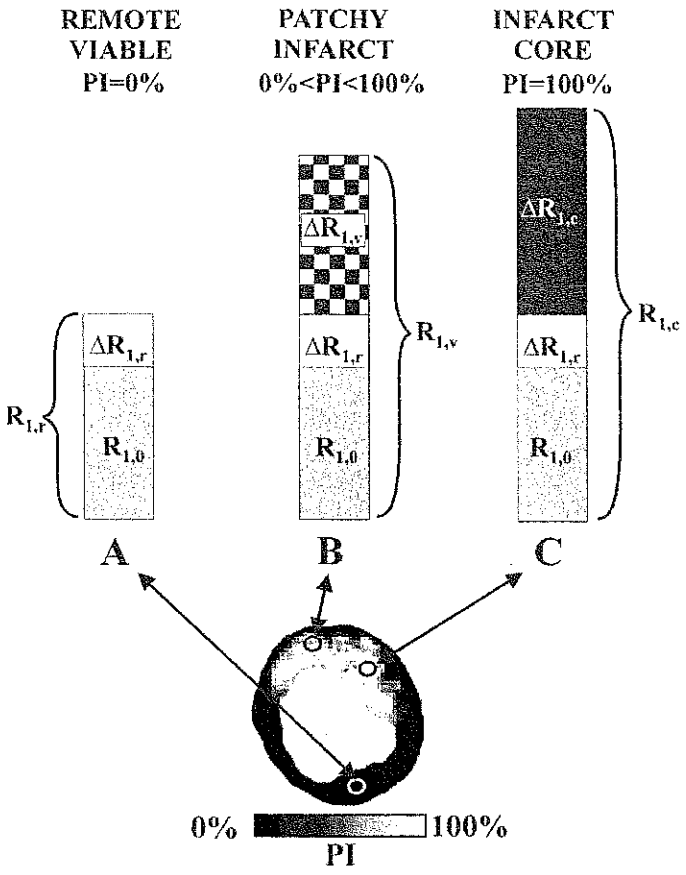

FIG. 1. Calculation of PI values is shown. R_1 is the relaxation rate measured in the presence of an infarct-avid CA. $R_{1,0}$ is measured in the absence of the CA. ΔR_1 is the relaxation rate enhancement induced by the CA. Examples of remote (**a**), partially infarcted (**b**), and completely infarcted (**c**) myocardial voxels are shown. $\Delta R_{1,r}$ is the baseline relaxation rate enhancement in all myocardial voxels due to the systemic administration of CA. $\Delta R_{1,c}$ is the relaxation rate enhancement, in addition to $\Delta R_{1,r}$, due to the infarct specificity and accumulation of the CA in 100% infarcted tissue (infarct core). $\Delta R_{1,v}$ is the relaxation rate enhancement in a voxel from a patchy infarct region. $\Delta R_{1,v}$ can range from zero to $\Delta R_{1,c}$. This dynamic range is the basis for the PI calculation. Bottom panel: voxel-by-voxel equatorial PIM with PI indicated on a heat-color scale.

dial contours of the LV muscle were traced manually using ImageJ (Wayne Rasband, NIH). In the long axis, the apical part of the LV, not covered by short-axis slices, was selected and included in the analysis. All further steps of the analysis were automated, which eliminated observer bias. The total LV myocardial mass (TMM) was determined by counting all myocardial pixels, and calculating the voxel mass (m_v) from the voxel size ($1.17 \cdot 1.17 \cdot 10$ mm^3) and myocardial specific gravity of 1.05 g/cm^3.

R_1 values were calculated pixel-by-pixel from the SI vs. TI dependence, applying three-parameter, nonlinear, least-squares curve-fitting (40,41):

$$SI = SI_0 \cdot (1 - A \cdot e^{(-TI \cdot R1)} + e^{(-TR \cdot R1)}) \quad [1]$$

where SI_0 and A are the SI at equilibrium, and a parameter ($A \leq 2$) that depends on the accuracy of the 180° inversion pulse, respectively. The last term of Eq. [1] ($e^{(-TR \cdot R1)}$) accounts for saturation, and was needed since we did not use a TR of five times T_1. Magnitude signal polarity was assigned as described by Nekolla et al. (42).

The relaxation rate R_1 ($R_1 \cong 1/T_1$) of each voxel was composed of $R_{1,0}$, the precontrast postinfarction control, i.e., the myocardial R_1 observed in the absence of the PCA, and ΔR_1, the contribution of the PCA present in the voxel:

$$R_1 = R_{1,0} + \Delta R_1 \quad [2]$$

Using Eq. [2], the R_1 map was transformed into a ΔR_1 map. The average $\Delta R_{1,r}$ value of areas remote from the infarct zone (about 600 voxels), was considered representative of 0% infarction:

$$\Delta R_{1,r} = R_{1,r} - R_{1,0} \quad [3]$$

The infarct-based ΔR_1 of each voxel, $\Delta R_{1,v}$ was obtained as follows:

$$\Delta R_{1,v} = R_{1,v} - R_{1,r} \quad [4]$$

As a threshold, $\Delta R_{1,v}$ of all remote voxels where $R_{1,v} < R_{1,r} + 2SD$, was set to zero.

After the area that displayed the largest ΔR_1 in the center of the infarct (5–10 voxels) was localized, its $\Delta R_{1,v}$ was chosen as representative of 100% infarction ($\Delta R_{1,c}$):

$$\Delta R_{1,c} = R_{1,c} - R_{1,r} \quad [5]$$

Solid infarcts in these regions were later confirmed postmortem by examining the corresponding regions on both sides of each of the three TTC-stained 3.3-mm slices. In all cases these regions were void of any viable tissue. Subsequently, a PI scale between 0% and 100% infarct was generated in terms of $\Delta R_{1,v}$ values. PI values were then calculated from $\Delta R_{1,v}$ values (Fig. 1):

Table 1
Mean (± SD) R_1 and ΔR_1 in Remote Regions (r) and Infarct Core (c)

	24 hr after PCA	48 hr after PCA
$R_{1,r}$	1.23 ± 0.06[a]	1.15 ± 0.08[b,c]
$R_{1,c}$	2.33 ± 0.5[d]	2.31 ± 0.4[d,c]
$\Delta R_{1,r}$	0.26 ± 0.03	0.18 ± 0.05
$\Delta R_{1,c}$	1.21 ± 0.5	1.27 ± 0.3

[a]Significantly different from $R_{1,c}$ at 24 hr after PCA ($P < 0.001$).
[b]Significantly different from $R_{1,c}$ at 48 hr after PCA ($P < 0.001$).
[c]Not significantly different from the same value at 24 hr after PCA.
[d]Significantly different from $R_{1,0}$ (0.98 s–1) ($P < 0.001$).

$$PI_v=(\Delta R_{1,v}/\Delta R_{1,c})\cdot 100 \quad [6]$$

where PI_v is the PI of a given voxel. Substituting $\Delta R_{1,v}$ from Eq. [4] and $\Delta R_{1,c}$ from Eq. [5], Eq. [6] becomes

$$PI_v=(R_{1,v}-R_{1,r})/(R_{1,c}-R_{1,r})\cdot 100 \quad [7]$$

Thus, the $R_{1,0}$ value was not needed for the calculation of PI values. The PI value for any voxel could be calculated from the actual $R_{1,v}$ using the actual postcontrast $R_{1,r}$ of remote, viable areas and the $R_{1,c}$ measured in the infarct core.

Color coding and the 3D reconstruction of the PIM were carried out using ImageJ. Thus, no sharp infarct contours were forced. The PI per slice (PIS_{PIM}) was determined by averaging all PI_v values in a given LV slice.

$$PIS_{PIM}=(\Sigma PI_v)/n_{slice}$$

(summation over all myocardial voxels in the slice) [8]

Where n_{slice} is the number of LV myocardial voxels in that slice.

The IF (IF_{PIM}) was calculated by averaging all PI_v values in a given LV:

$$IF_{PIM}=(\Sigma PI_v)/n_{LV}$$

(summation over all myocardial voxels in the LV) [9]

Where n_{LV} is the number of all LV myocardial pixels.

Additionally, we investigated whether the PIM method could be standardized by using the same universal remote R_1 limit (the mean $R_{1,r}$ of the six dogs; see Table 1) in all six dogs to define infarcted and noninfarcted myocardium. Using these universal $R_{1,r}$ values (one for the 24-hr and one for the 48-hr time point) we carried out the same calculations and analyses as above.

All analyses can be completed and the results obtained within an hour on a simple desktop computer. On more powerful workstations the entire procedure can be completed in a considerably shorter time frame.

Standard Measurement of Infarct Size Using SI Enhancement

At the 48-hr time point, additional standard IR-prepared images were acquired (using the same sequence as above) and the TI was chosen to null the signal arising from viable myocardial regions (hence we shall refer to these as DE-PCA). DE-PCA images were then analyzed using a threshold of Remote SI+2SD (15,43). To minimize observer bias, image analysis was semiautomated, with the only manual input being the tracing of endo-, and epicardial contours and the selection of a remote, viable region to determine the threshold.

In Vivo TTC Staining

Immediately following the acquisition of the 48-hr R_1 map, in vivo TTC staining was carried out (44). The in vivo staining method helps eliminate the distortion that occurs when TTC staining is done ex vivo after bread-slicing the heart. Following left anterolateral thoracotomy, 12.5 mL/kg saline with 2% TTC was administered I.V. For sufficient staining, TTC circulation was maintained for

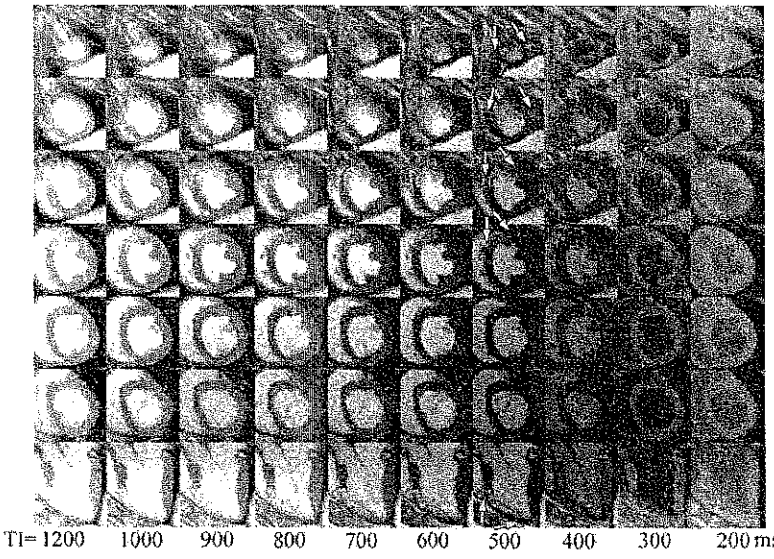

FIG. 2. IR images with varying TIs acquired 24 hr after PCA administration. Infarcted anteroseptal regions (due to transient LAD occlusion) with pronounced PCA accumulation are bracketed by arrows in the images obtained with TI = 500 ms, where remote myocardial signal was nulled.

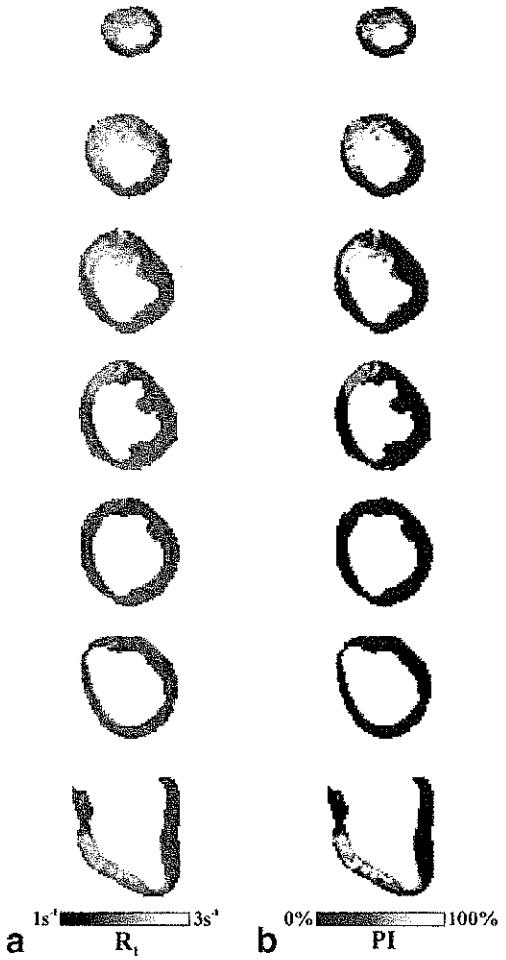

FIG. 3. **a:** Voxel-by-voxel R_1 maps generated from the images shown in Fig. 2. R_1 is shown on a grayscale. Higher R_1 values represent voxels in which a greater concentration of CA accumulates due to a higher percentage of infarcted tissue. **b:** The corresponding PIM. The higher the PI, the more severe the irreversible injury. Note that voxels with close to 100% infarct were mainly found subendocardially, while patchy infarct was mostly subepicardial and at the infarct borders, where salvage is most likely upon reperfusion.

20 min. Following euthanasia, the hearts were excised, perfused with saline to wash out blood, frozen by immersion in 95% ethanol at −80C°, and bread-sliced into 3.3-mm-thick short-axis slices. For each 10-mm slab of the myocardium, three 3.3-mm slices were obtained. Both sides of each TTC slice were photographed. Digital images were analyzed using ImageJ. Epi- and endocardial contours of the LV as well as infarcted areas were traced manually in all photos. Infarct mass in each TTC slice was determined by measuring and adding infarcted areas in the photos of both sides and multiplying them by half of the TTC slice thickness and by 1.05 g/cm^3. PIS_{TTC} was calculated by summing the infarct masses in three TTC slices that corresponded to an MRI slice and expressing it as a percentage of LV myocardial mass measured in the corresponding TTC slice. To obtain IF_{TTC}, results from all TTC photos were summed for each dog.

Statistical Analysis

The results are reported as the mean ± SD when the data sets passed both the normality and the equal variance tests. When the data sets did not pass either of these tests, the medians and percentiles are shown. Statistical analysis was carried out using SigmaStat 2.03 (SPSS, Inc). Two-way analysis of variance (ANOVA) was used to look for significant differences among R_1 values with respect to time (precontrast control, 24 hr, and 48 hr, after PCA) and region (infarct vs. viable). The Holm-Sidak all pairwise multiple comparison was carried out to identify significant differences among various time-points and regions. One-way ANOVA was used to compare TMM results among $PIM_{24\ hr}$, $PIM_{48\ hr}$ and TTC-staining. Pearson product moment correlation analyses were carried out pairwise between all MRI and TTC-staining results for PIS and IF. To compare each MRI method with TTC staining separately, the Mann-Whitney rank sum test was used to determine whether the results obtained with any of the methods were significantly different from those obtained with TTC staining. Dunn's method was used to compare measurement errors (overestimation above TTC) between $PIM_{24\ hr}$ and $PIM_{48\ hr}$. A P-value below 0.05 indicated statistical significance.

RESULTS

PIM

A representative set of IR images, acquired with multiple TIs, showing PCA-induced hyperenhancement in the multislice short-axis and three-chamber long-axis views is shown in Fig. 2. In Fig. 3, voxel-by-voxel R_1 maps (a) and PIMs (b) generated from such images are shown. The good quality and coregistration of images acquired with varying TI was confirmed by the R^2 values obtained for the pixel-by-pixel curve-fitting applied to the SI vs. TI dependence. The average R^2 in the myocardium was 0.99 ± 0.005.

FIG. 4. **a:** Standard IR-prepared image (TI = 500 ms) acquired 48 hr following PCA administration. Signal from remote, viable myocardium was completely nulled. **b:** Thresholded standard PCA-enhanced image generated from image a. All enhanced voxels are counted as 100% infarcted. **c:** Equatorial short-axis voxel-by-voxel PIM. PI is shown on a color scale with a range of 0–100% of infarcted tissue per voxel. **d:** The corresponding TTC-stained photo confirms that PIM localized the infarct accurately. The actual values for infarct size for this slice with the different techniques were: $PIS_{DE\text{-}PCA}$ = 47.5%; PIS_{TTC} = 28.9%; PIS_{PIM} = 28.3% (using individual $R_{1,r}$ values for the analysis). Although TTC staining shows only the surface of a slice, it confirms the tortuous morphology of the infarct and the residual viability subepicardially in the regions marked with arrows. In these regions infarcted and viable tissue are mixed. PIM visualizes the patchiness and quantified each voxel individually. Thus, PIM is a realistic representation of a tortuous infarct and yields an accurate measurement of overall infarct size.

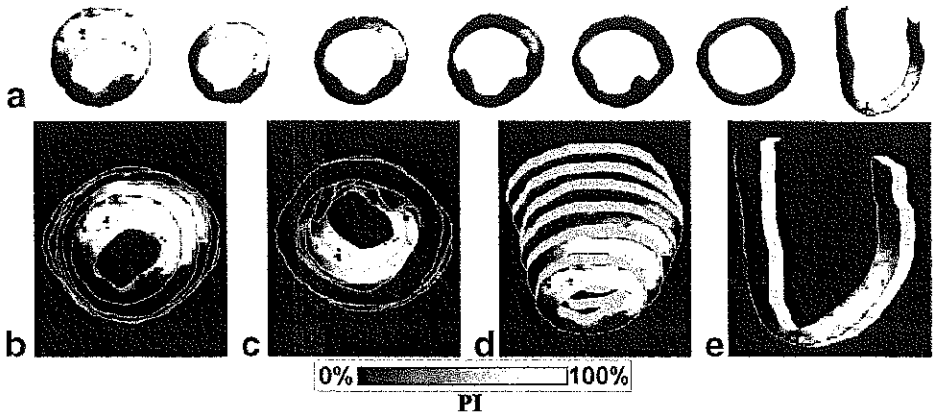

FIG. 5. **a:** Multislice short-axis and three-chamber long-axis PIMs 24 hr after PCA administration in a dog with anteroseptal infarction. **b–d:** 3D reconstruction of the LV viewed from the apex (b), base (c), and septum (d). **e:** Long-axis view.

The mean $R_{1,0}$ was 0.98 ± 0.05 s^{-1}, in agreement with other investigators' findings (35). The mean $R_{1,r}$, $\Delta R_{1,r}$, $R_{1,c}$, and $\Delta R_{1,c}$ for both time points post PCA are shown in Table 1. Interpolating from the 24- and 48-hr R_1 values, the hourly change in R_1 in all myocardial areas 24–48 hr post PCA was less than 1% of the measured R_1 (0.01 ± 0.3%/hr for infarcted and 0.26 ± 0.1%/hr for viable tissue), well below the experimental error of R_1 measurements. Thus we have confirmed that during generation of multislice R_1 maps covering the LV (30–40 min), the concentration of Gd(ABE-DTTA) does not change to an extent that would significantly interfere with the accuracy of R_1 measurement. This proves that Gd(ABE-DTTA) is a suitable PCA for multi-TI R_1 mapping.

PIM localized the infarct to the exact same territory as TTC staining. Equatorial short-axis PIM and a corresponding TTC slice are shown in Fig. 4. The TTC photos show information only on the "surface" of the slab, while PIM reflects data from the entire depth of the 10-mm-thick MRI slab and gives information about the tortuous shape of the infarct border zone. PIM, in agreement with TTC staining, detected partially viable ($0 < PI < 100$) regions along the infarct borders and in subepicardial, partially salvaged areas (indicated by arrows in Fig. 4.). Solid infarct regions were found (high PI values) subendocardially.

Figure 5 shows 3D reconstructions of short- and long-axis PIMs covering the entire LV. The changing fraction of infarcted cells can be observed with high in-plane spatial resolution, and in a graded manner.

No significant difference appeared between TMM determined using PIM at 24 hr (64 ± 5 g) or PIM at 48 hr (65 ± 4 g), and neither was significantly different from TMM_{TTC} (65 ± 5 g). Using individual remote R_1 limits, the mean ± SD total infarct mass values were 9.7 ± 3.7 g, 8.9 ± 3.5 g, and 9.4 ± 3.8 g for $PIM_{24\ hr}$, $PIM_{48\ hr}$, and TTC, respectively. These values correspond to the average $IF_{PIM24\ hr}$, $IF_{PIM48\ hr}$ (using individual remote R_1 limits), and IF_{TTC} values of 14.6% ± 5.7%, 12.8% ± 5.1%, and 13.8% ± 6.2%, respectively. The results obtained with the universal remote R_1 limits were not significantly different from those obtained with the individual limits (Table 2). Note that the large variability of the total infarct mass values was due to differences in infarct sizes among individual dogs, ranging from 3.1 to 13.1 g (as shown by TTC).

Using individual remote R_1 limits, significant pairwise correlations were found for $PIS_{PIM24\ hr}$ ($R = 0.97$, $P < 0.01$) and $PIS_{PIM48\ hr}$ ($R = 0.97$, $P < 0.01$), both vs. PIS_{TTC} (Table 3, Fig. 6). Also, strong significant correlations were obtained for $IF_{PIM24\ hr}$ ($R = 0.99$, $P < 0.01$) and $IF_{PIM48\ hr}$ ($R = 0.93$, $P < 0.01$) both vs. IF_{TTC} (Table 3). Median overestimations obtained with $PIM_{24\ hr}$ and $PIM_{48\ hr}$ as compared to TTC staining are shown in Table 3. PIS_{PIM} and IF_{PIM} at both time points were not significantly different from those obtained with TTC staining (P = NS).

The correlations and overestimation results (vs. TTC), obtained using the universal $R_{1,r}$ limits (Table 4), were similar to those obtained by using the individual $R_{1,r}$ limits. Slightly, but not significantly (P = NS), greater median deviations and similarly strong correlation coefficients were found vs. TTC staining.

Excellent correlation was obtained for $PIS_{PIM48\ hr}$ vs. $PIS_{PIM24\ hr}$ ($R = 0.97$, $P < 0.01$ using either individual or universal $R_{1,r}$). $PIS_{PIM24\ hr}$ and $IF_{PIM24\ hr}$ were slightly greater than those at 48 hr, on average by 1.6% ± 3.1% and 1.8% ± 1.6%, and by 3.1% ± 4.0% and −3.1% ± 2.6%, using individual and universal $R_{1,r}$, respectively. These

Table 2
Mean (± SD) Total Left Ventricular Myocardial Mass (TMM), Total Infarct Mass (TIM) Per Heart, and Infarction Fraction (IF) Values Obtained by Using the Different PIM Techniques at the Two Time-Points, and by TTC-Staining

Method	Time after PCA				
	PIM (individual)		PIM (universal)		TTC 48 hr
	24 hr	48 hr	24 hr	48 hr	
TMM (g)	64 ± 5	65 ± 4	64 ± 5	65 ± 4	65 ± 5
TIM (g)	9.7 ± 3.7	8.9 ± 3.5	10.3 ± 4.3	8.6 ± 3.3	9.4 ± 3.8
IF (%)	14.6 ± 5.7	12.8 ± 5.1	15.4 ± 7.2	12.2 ± 4.9	13.8 ± 6.2

Table 3
Median and 25th and 75th Percentile Overestimations of Infarct Sizes and Correlation Coefficients (R) Obtained for PIM (Using Individual Remote R_1 Limits) and for DE-PCA, Both vs. the Corresponding Values Obtained by TTC-Staining

	PIM		DE-PCA
	At 24 hr	At 48 hr	At 48 hr
Overestimation of PIS (%)			
Median	1.01	−0.53	29.7
25[a]	−2.45	−3.08	23.3
75[a]	1.98	0.79	32.9
Overestimation of IF (%)			
Median	1.23	0.49	22.2
25[a]	0.50	−2.78	21.9
75[a]	1.42	1.00	29.0
R for PIS	0.97*	0.97*	0.77**
R for IF	0.93*	0.99*	0.84**

[a]Percentile.
*$P < 0.01$.
**$P < 0.05$.

Table 4
Median and 25th and 75th Percentile Overestimations of Infarct Sizes and Correlation Coefficients (R) Obtained for PIM Using Universal Remote R_1 Limits and for DE-PCA, Both vs. TTC-Staining

	PIM		DE-PCA
	At 24 hr	At 48 hr	At 48 hr
Overestimation of PIS (%)			
Median	0.98	−1.83	29.7
25[a]	−1.88	−4.42	23.3
75[a]	3.14	0.58	32.9
Overestimation of IF (%)			
Median	1.05	−2.22	22.2
25[a]	0.20	−3.40	21.9
75[a]	2.71	−0.85	29.0
R for PIS	0.97*	0.96*	0.77**
R for IF	0.92*	0.89*	0.84**

[a]Percentile.
*$P < 0.01$.
**$P < 0.05$.

differences between the two time points for either PIS or IF, however, were not significant (P = NS), confirming the excellent reproducibility and stability of PIM.

Standard analysis of DE-PCA images at 48 hr (Fig. 4a and b) yielded significant overestimation of infarct size, and substantially weaker ($R = 0.77$ and $R = 0.84$ for $PIS_{DE\text{-}PCA}$ and $IF_{DE\text{-}PCA}$, respectively) but still significant ($P < 0.05$) correlations with TTC results (Table 3). The linear regression line for $PIS_{DE\text{-}PCA}$ vs. PIS_{TTC} yielded a slope of 1.4 and an intercept on the ordinate of 20.3. These results suggested substantial overestimation of true infarct size by the DE-PCA method. PIS_{TTC} and IF_{TTC} were overestimated by $PIS_{DE\text{-}PCA}$ and $IF_{DE\text{-}PCA}$ by a median of 29.7% and 22.2%, respectively (Table 3). Average remote and infarct SI values were 6.8% ± 1.8% and 50% ± 13% in the DE-PCA images, respectively. Remote SI was within 1 SD from the background noise of 5.8 ± 1.5, which confirmed successful nulling of signal from viable tissue.

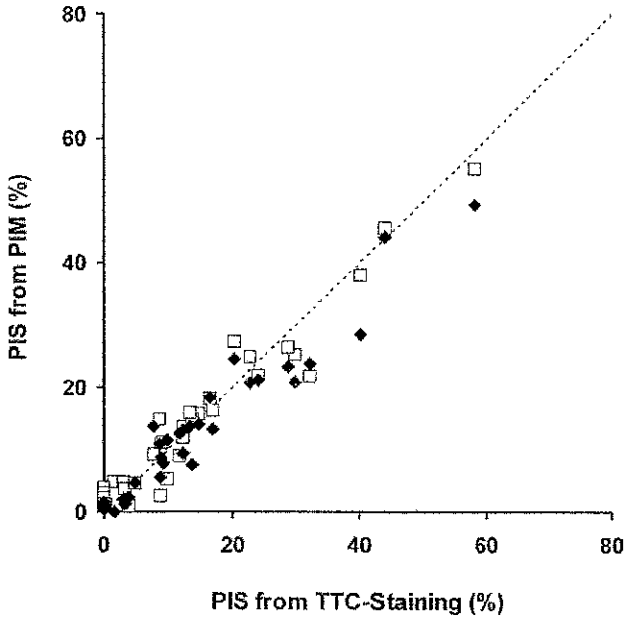

FIG. 6. Pairwise correlations in six dogs between PIS determined using $PIM_{24\ hr}$ (open squares) or $PIM_{48\ hr}$ (filled diamonds; using individual $R_{1,r}$ values for the analysis), both vs. TTC staining. Regression lines (not shown) were $y = 0.9x + 1.5$ ($R = 0.97$, $P < 0.01$), and $y = 0.83x + 0.9$ ($R = 0.97$, $P < 0.01$), for $PIM_{24\ hr}$ and $PIM_{48\ hr}$, respectively. The line of identity is shown as a dotted line. The PIS determined from PIM at either time point was not significantly different from the TTC results (P = NS).

DISCUSSION

We have shown that Gd(ABE-DTTA) accumulates in infarct, causing a persistent R_1 enhancement for 24–48 hr following administration. The slow clearance of this PCA allows generation of high-in-plane-resolution R_1 maps. We have shown that post PCA, a voxel-by-voxel ΔR_1 map of the entire LV can be generated, per-voxel PI values can be calculated, and a PIM can be constructed. In this manner the 3D information in MR images is used to quantify the severity and distribution (patchiness) of infarcts. Infarct size measurements (PIS_{PIM}, IF_{PIM}) obtained with in vivo PIM are in excellent agreement with those obtained with the histochemical gold standard, TTC staining (PIS_{TTC}, IF_{TTC}). The excellent correspondence between the results from PIM and those from TTC were mainly due to the R_1-based PIM analysis itself, as confirmed by the substantial overestimation of infarct size when DE-PCA images were acquired and analyzed using standard methods. Thus the advantage lies in the PIM method, rather than the particular CA (Gd(ABE-DTTA) used here.

The results obtained using the universal $R_{1,r}$ limits confirmed the possibility of eliminating observer bias even in the placing of a region of interest (ROI) to select a remote, viable myocardial region to provide the lower limit for $\Delta R_{1,r}$. Our results suggest that in human application, using the intrinsic R_1 parameter and the PIM method, it would be possible in the future (by means of large clinical trials) to establish universal R_1 limits for viable myocardium (for

any given CA), which would aid in the standardization of myocardial viability assessment.

The sensitivity of the PIM method can be calculated as follows: $\Delta R_{1,c}$ is the relaxation rate enhancement attributable to 100% infarction. Thus, if 1% of myocytes in a voxel were infarcted, the R_1 enhancement obtained relative to healthy areas would equal 0.0121 s^{-1} and 0.0127 s^{-1} at 24 hr and 48 hr, respectively. The typical error in R_1 arising from the noise in the images was 0.05 s^{-1} (the nonlinear least-squares fitting routine's estimate of uncertainty). This was comparable to but lower than the average SD of remote $R_{1,r}$ within individual experiments (0.06 s^{-1}). Since a 2 SD cutoff was used in our calculations to define PI = 0, infarcted tissue may have remained undetected only in voxels where PI $\leq$ 10% (2 · 0.06/0.0121) and PI $\leq$ 9% (2 · 0.06/0.0127), at 24 hr and 48 hr after PCA, respectively. In other words, only infarctions that affected less than 10% of cells in a voxel could have remained undetected with PIM. Thus, the threshold of infarct detection with PIM was 1.37 mm^3 (10% of voxel size).

It should be noted that fast proton exchange was not assumed for the entire voxel (1.17 × 1.17 × 10 mm^3), since R_1 is not averaged simply over the entire voxel. Rather, each minimal volume element (infarcted or noninfarcted tissue elements with different R_1 values) contributes to the net signal detected, resulting in multiexponential behavior of signal in regions where infarcted and viable tissue are mixed. The signal behavior for this particular range of R_1 values (corresponding to the entire range of PI values of 0–100%) approximates the signal behavior as if the measured monoexponential R_1 were the average R_1 of the individual relaxation rates of the different subvoxels, each with a distinct level of infarction. We carried out simulations (see Appendix) based on in vivo-observed R_1 values after PCA administration, using the TR and TI values employed in our experiments, to confirm that monoexponential fitting of multi exponentially simulated data does not yield curves of significantly worse quality than those resulting from multiexponential fitting for this range of R_1 values. The maximum R_1 error obtained was less than 1% (see Appendix and Fig. 7a), which is well within the experimental error of R_1 measurements. This error would translate into an error in the calculation of the voxel-by-voxel PI value, which is also negligible (see Appendix and Fig. 7b).

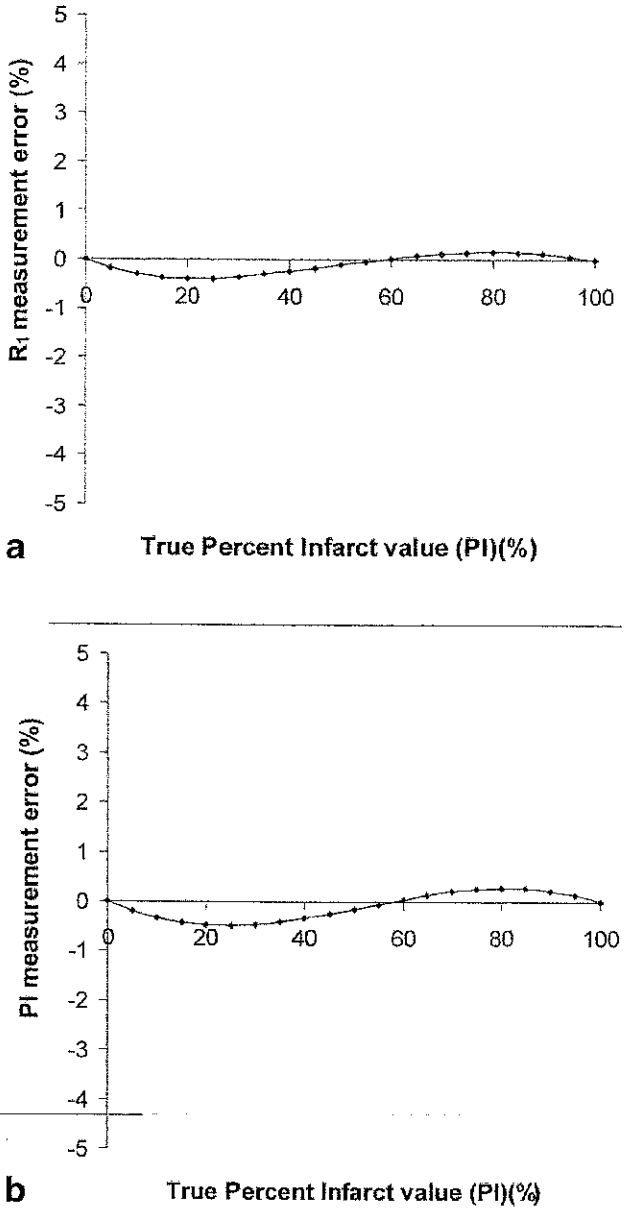

FIG. 7. **a:** Simulated error of R_1 measurement obtained by fitting Eq. [A1] (see Appendix), as opposed to fitting with Eq. [A2], for the entire range of PI values (0–100%). **b:** Simulated error of PI calculation resulting from fitting with Eq. [A1] (see Appendix), as opposed to fitting with Eq. [A2], for the entire range of PI values (0–100%).

We have shown that PIM is highly reproducible and timing-independent. The timing of R_1 mapping between 24 and 48 hr following PCA does not influence the infarct size measurements significantly. Although the 24-hr PIM and TTC were carried out 24 hr apart, this time span fell between 72 hr and 96 hr after reperfusion, a time period when infarct expansion was no longer under way and the infarct had not yet shrunk substantially. This conclusion was supported by the lack of significant change in TMM over this 24-hr period.

Potential differences in PCA clearance among individual dogs did not cause errors in infarct size determination because for each individual animal, at the time of examination, an individual relative scale was generated between ΔR_1 measured in the remote and infarct core areas. Although in this study only a small variability in the $\Delta R_{1,r}$ value was found, this was probably the result of the standardized experimental environment used for the different dogs (i.e., accurate dosing of CA, timing of image sessions), and the fact that all of the dogs were purpose-bred, healthy, and in the same weight range). Unfortunately, with patients in a clinical setting we can expect much greater variability among individuals due to varying extent of body fat or muscle mass, differences in kidney and/or liver function, etc. The residual concentration of CA in the remote regions may also vary with the timing of imaging following agent administration. Thus, generating a unique PI scale in terms of ΔR_1 values measured for each patient

will most likely be necessary for accurate infarct size determination.

Note also that PIM measurements would not be distorted in the event of a generalized myocardial disease. In patients with such a disease (e.g., concentric LV hypertrophy or dilated cardiomyopathy), $R_{1,0}$ would be uniformly altered in all myocardial voxels. Therefore, the associated $\Delta R_{1,\text{general-disease}}$, being equal in all voxels, would factor out from all of the foregoing equations. Although it is possible that a generalized disease would alter the relaxivity of the PCA, it would then be universally altered. Also, for such diseases, in large clinical trials, disease-specific R_1 limits could be established and used for infarct quantification. A generalized disease could also alter the behavior of infarcted tissue, and thus the infarct core $\Delta R_{1,c}$ could be somewhat different from that observed in the infarcts of otherwise healthy patients. However, this problem can be circumvented by measuring the infarct core ΔR_1 for these particular patients individually.

There are several reasons for the relative high accuracy and reproducibility of PIM. In the course of the three-parameter curve-fitting, R_1 values, contrary to SI, are insulated from many extraneous experimental factors. Using PIM, the need to categorize voxels (represented by pixels) into two groups of viable vs. nonviable voxels by means of a thresholding method is eliminated. Also, determination of infarct contours is not necessary with this method. Since PIM quantifies infarct patchiness per voxel and highlights each voxel proportionately to the amount of irreversible tissue it contains, a more graded infarct-distribution map can be obtained. There appears to be a significant advantage in having a direct and accurate measurement of the subvoxel % infarction. PIM, therefore, provides in-depth quantification of infarcts, and is superior in this respect even to TTC staining, since TTC staining reveals only the surface of a given slice. With PIM, masking of viable areas by infarcted tissue islets (in areas of patchy infarct due to partial volume effects), is eliminated, and otherwise undetected viable tissue is revealed.

In the present study no major microvascular obstruction was detected in the form of large unenhanced regions in the center of the infarcts. This may reflect the long tissue lifetime of the PCA, which allowed enough time for the PCA to access even no-reflow regions via diffusion. Nevertheless, when applying the PIM method using a CA with fast kinetics, regions of microvascular obstruction will likely present as regions in the center of the infarct that display decreased PI values.

Two drawbacks of PCA-PIM are the time needed to acquire accurate R_1 maps, and that the fact that agents currently approved for clinical use have fast tissue kinetics. Both problems, however, will likely be circumvented in the near future. Respiratory navigator techniques could eliminate the need for breath-holds, and automated "built-in" packages with multiple readout sequences could generate PIMs of the heart in a reasonable time frame, even for CAs with fast tissue kinetics. Also, a fast R_1-mapping approach was recently demonstrated by Messroghli et al. (35), who showed the feasibility of IR-based R_1 mapping in patients. We wish to emphasize that the PIM method is not dependent on the use of a particular CA. Any infarct-avid agent can be used for this purpose once such fast R_1-mapping methods become commercially available. Since R_1 is an intrinsic parameter, any sequence could be used (as long as it yields accurate R_1 values) to generate the R_1 map, from which the PIM is calculated. Thus, PIM has the potential to help standardize multicenter studies, and improve comparability and reproducibility of myocardial viability assessment with CE-MRI.

APPENDIX

Each imaged voxel consists of subvoxels, which by definition are of a size such that due to fast proton exchange, R_1 values are truly averaged. These subvoxels in the myocardium are either infarcted (necrotic myocytes that accumulate the CA) or viable (non-accumulating). The signal detected in any voxel is the sum total of the signal contributions from all the subvoxels from within the voxel. Myocardial voxels in the infarct core consist of all infarcted subvoxels (all sharing the same $R_{1,c}$), whereas remote, viable voxels consist of all viable subvoxels ($R_{1,r}$). For both types of voxels, the image intensity in our IR sequence can be described as:

$$SI = SI_0 \cdot (1 - A \cdot e^{(-TI \cdot R1)} + e^{(-TR \cdot R1)}) \qquad [A1]$$

using either $R_{1,c}$ or $R_{1,r}$ for R_1. For the voxels containing a mixture of infarcted and noninfarcted subvoxels (i.e., $0 < PI < 100\%$), and where fast proton exchange cannot be assumed, the image intensity will vary as:

$$SI = SI_0 \cdot (F_c \cdot (1 - A \cdot e^{(-TI \cdot R1c)} + e^{(-TR \cdot R1c)}) + F_r \cdot (1 - A \cdot e^{(-TI \cdot R1r)} + e^{(-TR \cdot R1r)})) \qquad [A2]$$

where F_c and F_r represent the percentage of infarcted and noninfarcted subvoxels in a given voxel, respectively. However, if the signal from these voxels is fitted using Eq. [A1], assuming that R_1 is able to be averaged, one would expect a systematic error to be introduced into R_1 and thus into the PI value calculated.

Using Eq. [A2], and based on experimentally determined $R_{1,c}(2.3\ s^{-1})$ and $R_{1,r}(1.15\ s^{-1})$ values and a TR of 2000 ms, we simulated the SI values at 10 different TI values (in the range of 100–1000 in steps of 100 ms) from voxels that consisted of varying proportions of infarcted vs. viable subvoxels (PI varied from 0 to 100 in steps of 5%). For the simulations the parameter values $A = 2$, $SI_0 = 1$, $F_c = PI/100$ and $F_r = (100 - PI/100)$ were used.

Based on the above multiexponentially simulated signal intensities, apparent $R_{1,app}$ values were determined by monoexponential curve-fitting using Eq. [A1]. The apparent PI_{app} value was then calculated as detailed in the Materials and Methods section. The theoretical average $R_{1,av}$ for each of the simulated voxels was calculated using the values of PI, $R_{1,c}$, and $R_{1,r}$. The error in $R_{1,app}$ compared to $R_{1,av}$ as a function of PI is shown in Fig. 7a. Figure 7b shows the effect of these small errors on the calculation of PI. Both $R_{1,app}$ and PI_{app} were within 1% of the theoretically calculated values. This confirms that using Eq. [A1] to fit data from noncommunicating subvoxels does not lead to significant errors in determining R_1, and thus PI values can be determined accurately. This relationship can

be described, similarly to the R_1-averaging present in fast exchange, by the following equation:

$$<R_1> = F_c \cdot R_{1,c} + F_r \cdot R_{1,r} \quad [A3]$$

Where $<R_1>$ stands for the average R_1 observed in the voxel.

ACKNOWLEDGMENTS

This study was supported by grants from the NIH to P.S. (R44 HL58285) and G.A.E. (RO1 HL63340).

REFERENCES

1. Beller GA. Noninvasive assessment of myocardial viability. N Engl J Med 2000;343:1487–1490.
2. Wagner A, Mahrholdt H, Holly TA, Elliott MD, Regenfus M, Parker M, Klocke FJ, Bonow RO, Kim RJ, Judd RM. Contrast-enhanced MRI and routine single photon emission computed tomography (SPECT) perfusion imaging for detection of subendocardial myocardial infarcts: an imaging study. Lancet 2003;361:374–379.
3. Travin M, Bergmann S. Assessment of myocardial viability. Semin Nucl Med 2005;35:2–16.
4. Balcells E, Powers ER, Lepper W, Belcik T, Wei K, Ragosta M, Samady H, Lindner JR. Detection of myocardial viability by contrast echocardiography in acute infarction predicts recovery of resting function and contractile reserve. J Am Coll Cardiol 2003;41:827–833.
5. Kim RJ, Wu E, Rafael A, Chen EL, Parker MA, Simonetti O, Klocke FJ, Bonow RO, Judd RM. The use of contrast-enhanced magnetic resonance imaging to identify reversible myocardial dysfunction. N Engl J Med 2000;343:1445–1453.
6. Simonetti OP, Kim RJ, Fieno DS, Hillenbrand HB, Wu E, Bundy JM, Finn JP, Judd RM. An improved MR imaging technique for the visualization of myocardial infarction. Radiology 2001;218:215–223.
7. Hillenbrand HB, Kim RJ, Parker MA, Fieno DS, Judd RM. Early assessment of myocardial salvage by contrast-enhanced magnetic resonance imaging. Circulation 2000;102:1678–1683.
8. Choi SH, Lee SS, Choi SI, Kim ST, Lim KH, Lim CH, Weinmann H-J, Lim T-H. Occlusive myocardial infarction: investigation of bis-gadolinium mesoporphyrins-enhanced T1-weighted MR imaging in a cat model. Radiology 2001;220:436–440.
9. Gerber BL, Garot J, Bluemke DA, Wu KC, Lima JA. Accuracy of contrast-enhanced magnetic resonance imaging in predicting improvement of regional myocardial function in patients after acute myocardial infarction. Circulation 2002;106:1083–1089.
10. Kuhl HP, Beek AM, van der Weerdt AP, Hofman MB, Visser CA, Lammertsma AA, Heussen N, Visser FC, van Rossum AC. Myocardial viability in chronic ischemic heart disease: comparison of contrast-enhanced magnetic resonance imaging with (18)F-fluorodeoxyglucose positron emission tomography. J Am Coll Cardiol 2003;41:1341–1348.
11. Watzinger N, Lund GK, Higgins CB, Wendland MF, Weinmann HJ, Saeed M. The potential of contrast-enhanced magnetic resonance imaging for predicting left ventricular remodeling. J Magn Reson Imaging 2002;16:633–640.
12. Klein C, Nekolla S, Bengel F, Momose M, Sammer A, Haas F, Schnackenburg B, Delius W, Mudra H, Wolfram D, Schwaiger M. Assessment of myocardial viability with contrast-enhanced magnetic resonance imaging: comparison with positron emission tomography. Circulation 2002;105:162–167.
13. Kramer C, Rogers W, Mankad S, Theobald T, Pakstis D, Hu Y. Contractile reserve and contrast uptake pattern by magnetic resonance imaging and functional recovery after reperfused myocardial infarction. J Am Coll Cardiol 2000;36:1835–1840.
14. Rochitte CE, Lima JAC, Bluemke DA, Reeder SB, McVeigh ER, Furuta T, Becker LC, Melin JA. Magnitude and time course of microvascular obstruction and tissue injury after acute myocardial infarction. Circulation 1998;98:1006–1014.
15. Kim RJ, Fieno DS, Parrish TB, Harris K, Chen EL, Simonetti O, Bundy J, Finn JP, Klocke FJ, Judd RM. Relationship of MRI delayed contrast enhancement to irreversible injury, infarct age, and contractile function. Circulation 1999;100:1992–2002.
16. Judd RM, Lugo-Olivieri CH, Arai M, Kondo T, Croisille P, Lima JA, Mohan V, Becker LC, Zerhouni EA. Physiological basis of myocardial contrast enhancement in fast magnetic resonance images of 2-day-old reperfused canine infarcts. Circulation 1995;92:1902–1910.
17. Saeed M, Bremerich J, Wendland MF, Wyttenbach R, Weinmann H-J, Higgins CB. Reperfused myocardial infarction as seen with use of necrosis-specific vs. standard extracellular MR contrast media in rats. Radiology 1999;213:247–257.
18. Saeed M, Lund G, Wendland MF, Bremerich J, Weinmann H, Higgins CB. Magnetic resonance characterization of the peri-infarction zone of reperfused myocardial infarction with necrosis-specific and extracellular nonspecific contrast media. Circulation 2001;103:871–876.
19. Oshinski JN, Yang Z, Jones JR, Mata JF, French BA. Imaging time after Gd-DTPA injection is critical in using delayed enhancement to determine infarct size accurately with magnetic resonance imaging. Circulation 2001;104:2838–2842.
20. Grebe O, Paetsch I, Kestler H, Herkommer B, Schnackenburg B, Hombach V, Fleck E, Nagel E. Optimal acquisition parameters for contrast enhanced magnetic resonance imaging after chronic myocardial infarction. J Cardiovasc Magn Reson 2003;5:575–587.
21. Amado LC, Gerber BL, Gupta SN, Rettmann DW, Szarf G, Schock R, Nasir K, Kraitchman DL, Lima JAC. Accurate and objective infarct sizing by contrast-enhanced magnetic resonance imaging in a canine myocardial infarction model. J Am Coll Cardiol 2004;44:2383–2389.
22. Ibrahim T, Nekolla SG, Hornke M, Bulow HP, Dirschinger J, Schomig A, Schwaiger M. Quantitative measurement of infarct size by contrast-enhanced magnetic resonance imaging early after acute myocardial infarction: comparison with single-photon emission tomography using Tc99m-sestamibi. J Am Coll Cardiol 2005;45:544–552.
23. Setser R, Bexell D, O'Donnell T, Stillman A, Lieber M, Schoenhagen P, White R. Quantitative assessment of myocardial scar in delayed enhancement magnetic resonance imaging. J Magn Reson Imaging 2003;18:434–441.
24. Fritz-Hansen T, Rostrup E, Ring PB, Larsson HB. Quantification of gadolinium-DTPA concentrations for different inversion times using an IR-turbo flash pulse sequence: a study on optimizing multislice perfusion imaging. Magn Reson Imaging 1998;16:893–899.
25. Messroghli D, Niendorf T, Schulz-Menger J, Dietz R, Friedrich M. T1 mapping in patients with acute myocardial infarction. J Cardiovasc Magn Reson 2003;5:353–359.
26. Simor T, Chu WJ, Johnson L, Safranko A, Doyle M, Pohost GM, Elgavish GA. In vivo MRI visualization of acute myocardial ischemia and reperfusion in ferrets by the persistent action of the contrast agent Gd (BME-DTTA). Circulation 1995;92:3549–3559.
27. Saab-Ismail NH, Simor T, Gaszner B, Lorand T, Szollosy M, Elgavish GA. Synthesis and in vivo evaluation of new contrast agents for cardiac MRI. J Med Chem 1999;42:2852–2861.
28. Kim SK, Pohost GM, Elgavish GA. Gadolinium complexes of [(myristoyloxy) propyl]diethylenetriaminetetraacetate: new lipophilic, fatty acyl conjugated NMR contrast agents. Bioconj Chem 1992;3:20–26.
29. Kim SK, Pohost GM, Elgavish GA. Fatty-acyl iminopolycarboxylates: lipophilic bifunctional contrast agents for NMR imaging. Magn Reson Med 1991;22:57–67.
30. Chu WJ, Elgavish GA. Gadolinium and dysprosium chelates of DTPA-amide-dextran: synthesis, 1H NMR relaxivity, and induced 23Na NMR shift. NMR Biomed 1995;8:159–163.
31. Chu WJ, Simor T, Elgavish GA. In vivo characterization of Gd(BME-DTTA), a myocardial MRI contrast agent: tissue distribution of its MRI intensity enhancement, and its effect on heart function. NMR Biomed 1997;10:87–92.
32. Surányi P, Kiss P, Brott BC, Simor T, Elgavish A, Elgavish GA. Determining tissue kinetics of Gd(ABE-DTTA), an infarct-avid, persistent contrast-agent in canine myocardial infarction. In: Proceedings of the 12th Annual Meeting of ISMRM, Kyoto, Japan, 2004. p 1836.
33. Simor T, Gaszner B, Oshinski J, Waldrop S, Pettigrew R, Horvath I, Hild G, Elgavish G. Gd(ABE-DTTA)-enhanced cardiac MRI for the diagnosis of ischemic events in the heart. J Magn Reson Imaging 2005;21:536–545.
34. Surányi P, Kiss P, Brott BC, Simor T, Elgavish A, Elgavish GA. Repeated, pixel-by-pixel T1-mapping in canine myocardial infarction, using an infarct-avid, persistent contrast agent, Gd(ABE-DTTA). In: Proceedings of the 12th Annual Meeting of ISMRM, Kyoto, Japan, 2004. p 172.

35. Messroghli D, Radjenovic A, Kozerke S, Higgins D, Sivananthan M, Ridgway J. Modified Look-Locker inversion recovery (MOLLI) for high-resolution T1 mapping of the heart. Magn Reson Med 2004;52:141–146.
36. Fishbein M, Meerbaum S, Rit J, Lando U, Kanmatsuse K, Mercier J, Corday E, Ganz W. Early phase acute myocardial infarct size quantification: validation of the triphenyl tetrazolium chloride tissue enzyme staining technique. Am Heart J 1981;101:593–600.
37. Choi S, Jiang C, Lim K, Kim S, Lim C, Gong G, Lim T. Application of breath-hold T2-weighted, first-pass perfusion and gadolinium-enhanced T1-weighted MR imaging for assessment of myocardial viability in a pig model. J Magn Reson Imaging 2000;11:476–480.
38. Weiss CR, Aletras AH, London JF, Taylor JL, Epstein FH, Wassmuth R, Balaban RS, Arai AE. Stunned, infarcted, and normal myocardium in dogs: simultaneous differentiation by using gadolinium-enhanced cine MR imaging with magnetization transfer contrast. Radiology 2003;226: 723–730.
39. Kiss P, Simor T, Lenard L, Hejjel L, Suranyi P, Saab-Ismail NH, Elgavish GA. Relaxivity of Gd.(ABE-DTTA) increases with magnetic field strength up to 5T. A contrast agent for high field imaging. In: Proceedings of the 10th Annual Meeting of ISMRM, Honolulu, HI, USA, 2002. p 10.
40. Canet D, Levy GC, Peat IR. Time saving in ^{13}C spin-lattice relaxation measurements by inversion-recovery. J Magn Reson 1975;18:199–204.
41. Kaldoudi E, Williams SCR. Relaxation time measurements in NMR imaging. Part I: Longitudinal relaxation time. Concepts Magn Reson 1993;5:217–242.
42. Nekolla S, Gneiting T, Syha J, Deichmann R, Haase A. T1 maps by k-space reduced snapshot-FLASH MRI. J Comput Assist Tomogr 1992; 16:327–332.
43. Dewey M, Kaufels N, Laule M, Schnorr J, Wagner S, Kivelitz D, Raynaud J, Robert P, Hamm B, Taupitz M. Assessment of myocardial infarction in pigs using a rapid clearance blood pool contrast medium. Magn Reson Med 2004;51:703–709.
44. Fallon J. Postmortem: histochemical techniques. In: GS W, editor. Myocardial infarction: measurement and intervention. Boston: Martinus Nijhoff Publishers; 1982. p 373–384.